Dalton Transactions



PAPER

View Article Online
View Journal | View Issue



Cite this: *Dalton Trans.*, 2025, **54**, 11551

Sterically hindered P,N-type amidophosphines $\{(o-PPh_2)C_6H_4\}C(O)NH(R)\}$: synthesis, transition metal chemistry, and catalytic activity in stereoselective Heck coupling of aryl chlorides†

Gazal Sabharwal, (D) Khilesh C. Dwivedi (D) and Maravanji S. Balakrishna (D) *

This paper reports the synthesis, coordination chemistry, and catalytic applications of two amide-based monophosphine ligands, $\{((o-PPh_2)C_6H_4)C(O)N(H)(C_{12}H_{18})\}$ (L1) and $\{((o-PPh_2)C_6H_4)C(O)NH(C_{33}H_{28})\}$ (L2). Ligand L1, upon reaction with $[Pd(COD)Cl_2]$ and $[Pd(OAc)_2]$, yielded dimeric P,N-coordinated palladium complexes $[\{(PdCl)_2\}\{(o-PPh_2)C_6H_4C(O)N(C_{12}H_{18})\}_2-\kappa^2-P,N]$ (1) and $[\{(Pd(OAc))_2\}\{(o-PPh_2)C_6H_4C(O)N(C_{12}H_{18})\}_2-\kappa^2-P,N]$ (2), respectively. Further treatment of L1 with Cul and AgBr afforded monodentate \mathfrak{n}^1 -P coordinated copper and silver complexes, $[\{(Cul)_2\}\{(o-PPh_2)C_6H_4C(O)NH(C_{12}H_{18})\}_2-\kappa^1-P]$ (3) and $[\{(AgBr)_2\}\{(o-PPh_2)C_6H_4C(O)N(H)(C_{12}H_{18})\}_2-\kappa^1-P]$ (4). Reactions of L1 with AgBF4 and AgClO4 led to the formation of tridentate P,O,C-coordinated silver complexes, namely $[\{(AgX)_2\}\{(o-PPh_2)C_6H_4C(O)N(H)(C_{12}H_{18})\}_2-\kappa^3-P,O,C]$, where $X=BF_4$ (5) and CIC_4 (6). Ligand L2 reacted with Cul to form a monodentate P-coordinated Cu¹ complex, $[\{(Cul)_2\}\{(o-PPh_2)C_6H_4C(O)NH(C_{33}H_{28})\}_2-\kappa^1-P]$ (8), and with $[Ru(p-cymene)Cl_2]_2$ to afford a P,O-chelated Ru¹¹ complex, $[\{Ru(p-cymene)Cl_3\{(o-PPh_2)C_6H_4C(O)NH(C_{33}H_{28})\}_2-\kappa^2-P,O]$ PF6 (9). Notably, the *in situ*-generated Pd nanoparticles derived from complex 1, stabilized by the P,N ligand, exhibited excellent catalytic performance in Heck cross-coupling reactions of aryl chlorides with styrene derivatives. These reactions proceed under mild conditions, providing *trans*-stilbene products in high yields (90–99%) with low catalyst loading and good functional group tolerance.

Received 9th June 2025, Accepted 9th July 2025 DOI: 10.1039/d5dt01353d

rsc.li/dalton

Introduction

Ligand design is central to advancing coordination chemistry and transition metal catalysis, with tertiary phosphines (PR₃) standing out for their ability to finely tune the electronic and steric environment of metal centres. Phosphine ligands incorporating nitrogen donor groups (P,N-ligands) are particularly valuable due to their hemilabile nature, combining soft phosphorus and hard nitrogen donors. His duality allows for dynamic coordination behaviour: the nitrogen donor can reversibly dissociate to create vacant coordination sites, while the chelating interaction stabilizes the complex in the absence of substrate. The performance of P,N-ligands is further enhanced by their electronic asymmetry and steric versatility. Incorporating additional heteroatoms or sterically demanding substituents increases both the stability and reactivity of metal

Phosphorus Laboratory, Department of Chemistry, Indian Institute of Technology Bombay, Powai, Mumbai 400076, India. E-mail: krishna@chem.iitb.ac.in, msb_krishna@iitb.ac.in; Fax: +91-22-5172-3480/2576-7152

†Electronic supplementary information (ESI) available. CCDC 2456488-2456497. For ESI and crystallographic data in CIF or other electronic format see DOI: https://doi.org/10.1039/d5dt01353d

complexes, enabling efficient catalysis across a broad range of transformations. 13-19 Notably, phosphines bearing pendant aromatic groups adjacent to phosphorus exhibit diverse coordination modes ($\eta^2 - \eta^6$), contingent on the metal's electronic state, thus offering further tunability in catalytic systems. 20-24 In particular, amide-derived phosphines present an attractive platform, owing to the inherent coordinating properties of the amide moiety and the ease of structural modification at the nitrogen center, which facilitates the incorporation of diverse steric and electronic features.²⁵ Despite extensive studies on conventional P,N- and P,O-type ligands, 26-28 the class of aromatic amide-based monophosphines featuring dangling tertiary amide groups remains relatively underexplored. The introduction of dynamic steric hindrance via bulky N-aryl or N-alkyl substituents provides an opportunity to modulate ligand flexibility and metal coordination geometry, potentially facilitating key steps in catalytic cycles such as substrate coordination, oxidative addition, and reductive elimination.29 While related P. N-ligands and amido-phosphines have been reported in the literature, 30-32 the use of aromatic amide-derived monophosphines with bulky N-substituents and their ability to support a range of coordination modes (P,P,N, P,O,C) across multiple metals (Pd, Cu, Ag, Ru) remains underexplored.

Paper **Dalton Transactions**

Palladium plays a central role in transition metal catalysis due to its broad functional group tolerance, mild reaction conditions, and capacity to activate a variety of bonds, including C-H, C-X (X = Cl, Br, I), and C-Sn. $^{33-37}$ Its catalytic efficiency is markedly improved through coordination with electron-rich ligands, especially phosphines, which enhance the electron density at the metal center and promote key steps in the catalytic cycle. 38-40

Palladium nanoparticles (Pd NPs) stabilized by various ligands under mild conditions have garnered significant attention in recent years due to their catalytic potential. 41-45 Phosphorus-based ligands, in particular, have been employed as surfactants to effectively stabilize Pd NPs. 17,46-48 Notably, in situ-generated palladium nanoparticles prepared under milder and less hazardous conditions have demonstrated superior catalytic activity compared to their corresponding molecular complexes, while also offering a more cost-effective alternative. 43,49-52

The palladium-catalyzed arylation of olefins with aryl halides, widely known as the Heck reaction, has garnered considerable interest over the past decade for its broad applicability in carbon-carbon bond formation. 53-61 It is pivotal in synthesizing key intermediates for the pharmaceutical and chemical industries. 62,63 Beyond conventional aryl halides, alternative aryl sources such as aryl triflates, diazonium salts, sulfonyl halides, and aroyl halides, have been explored, along with the development of highly efficient catalytic systems.^{64–67}

However, industrial application remains limited, particularly with chloroarenes, despite their low cost and availability. The Heck coupling reaction continues to face significant challenges, including high catalyst loadings (1-5 mol%), elevated reaction temperatures (>130 °C), dependence on additives, reducing agents, or phase-transfer catalysts, as well as limitations in selectivity and overall efficiency, underscoring the need for more active, selective, and practical catalytic systems. 68,69

Sasson and co-workers, reported significant side reactions, including double bond hydrogenation, styrene reduction to ethylbenzene, homocoupling, and hydrodehalogenation, when using equimolar haloarene and styrene with high loading of Pd/C, PEG-400, sodium formate, and base. 70 Xu and coworkers achieved trans-Heck products from aryl chlorides and olefins using n-Bu₄N⁺OAc⁻ as base, but only under high palladium and ligand loadings. 71 Beller and co-workers developed a cyclometallated PdII complex that enabled coupling of aryl bromides with *n*-butyl acrylate at low catalyst loadings; however, the method required elevated temperatures and prolonged reaction times (Scheme 1).72 Recently Madrahimov and coworkers, have demonstrated the heterogenization of mono (phosphine)-Pd complexes on UiO-66 MOF surfaces for Heck reactions, achieving moderate yields (40-92%) but requiring high catalyst loadings.⁷³ Similarly, Gevorgyan and co-workers developed a visible-light-induced Pd-catalyzed Heck coupling of oximes with alkyl halides, though the method suffered from

Scheme 1 Heck-coupling reaction reported by various groups.

Dalton Transactions Paper

high catalyst loadings, limited scope (ineffective for chloro derivatives), and formation of cis/trans mixtures. 74 Strassner and co-workers employed tunable aryl alkyl ionic liquids (TAAILs) at elevated temperatures (140 °C), with high Pd loadings, to couple bromobenzene and styrene, again producing trans-stilbene.75

To overcome existing limitations in Heck coupling, we present a novel amido-phosphine ligand and its dimeric P.Ncoordinated PdII complex, which efficiently catalyses the arylation of styrene derivatives with aryl chlorides under mild conditions. Operating at low catalyst loadings, the system delivers trans-stilbene products in excellent yields (90-99%) with broad substrate scope and high selectivity. This study demonstrates how the hemilabile, flexible nature of the ligand framework can be exploited to design efficient and sustainable catalysts for C-C bond-forming transformations.

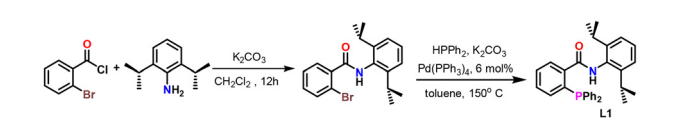
Results and discussion

Synthesis of amide based monophosphine ligand: N-(2,6diisopropylphenyl)-2-(diphenylphosphaneyl)benzamide (L1)

The reaction of 2,6-diisopropylaniline with 2-bromobenzoyl chloride in 1:1 molar ratio afforded the corresponding amide in quantitative yield. Subsequent treatment with 1.3 equivalents of diphenylphosphine in the presence of catalytic amount of [Pd(PPh₃)₄] and K₂CO₃ furnished the monophosphine ligand L1 in high yield (Scheme 2).76,77 The structure of L1 was confirmed by NMR, mass, IR spectroscopy, and singlecrystal X-ray analysis. In the ¹H NMR spectrum, the NH proton appeared at 7.95 ppm, while the ¹³C{¹H} NMR spectrum showed the amide carbonyl carbon at 168.8 ppm. Aromatic proton resonances were observed in the range 7.00-7.80 ppm. The IR spectrum exhibited characteristic absorptions at 3364 cm⁻¹ (N-H stretch) and 1653 cm⁻¹ (C=O stretch). Crystals suitable for X-ray diffraction were obtained from dichloromethane, and the molecular structure is depicted in Fig. 1, with selected bond lengths (Å) and angles (°) mentioned in the figure caption.

Synthesis of PdII, CuI and AgI complexes

The reactions of ligand L1 with [Pd(COD)Cl₂] and [Pd(OAc)₂] in 1:1 ratio, in dichloromethane afforded the complexes $[{(PdCl)_2}{\{(o-PPh_2)C_6H_4\}C(O)N(C_{12}H_{18})\}_2-\kappa^2-P,N}]$ $[\{(CH_3C(O)O)(Pd)_2\}\{\{(o-PPh_2)C_6H_4\}C(O)N(C_{12}H_{18})\}_2-\kappa^2-P,N]$ (Scheme 3) in good yields as intense yellow colour solids. In the IR spectra of both the complexes the N-H stretching frequency disappears. In case of complex 2, carbonyl stretching frequency appeared at 1549 cm⁻¹ and the C-O stretching fre-



Scheme 2 Synthesis of L1.

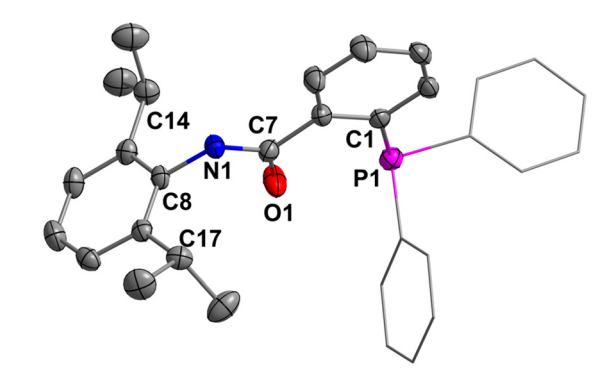


Fig. 1 Single X-ray crystal structure of ligand L1. All hydrogen atoms have been omitted for clarity. Displacement ellipsoids are drawn at 50% probability level. Selected bond lengths [Å] and bond angles [°]: P1-C1 1.868(2), C7-O1 1.236(2), N1-C7 1.355(3), NI-C7-O1 121.8(2).



Scheme 3 Synthesis of PN-Pd^{II} complexes 1 and 2.

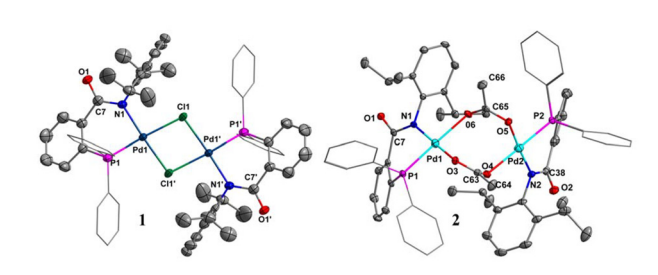


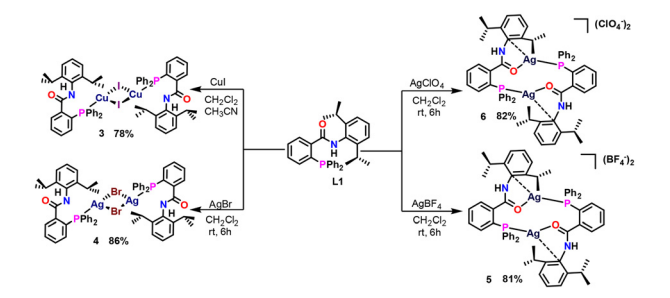
Fig. 2 Single X-ray crystal structure of complexes 1 and 2. All hydrogen atoms have been omitted for clarity. Displacement ellipsoids are drawn at 50% probability level.

quency appears at 1099 cm⁻¹. The crystal structures of both the complexes are shown in Fig. 2, with selected bond lengths and bond angles mentioned in Table 1. Complexes 1 and 2 are both dinuclear, with palladium centers adopting distorted square planar geometries. Complex 1 features chloride bridges, forming two six-membered and one four-membered metallacycles, whereas complex 2 contains acetate bridges, leading to the formation of two six-membered and one eightmembered metallacycles.

The reaction of ligand L1 with CuI in 1:1 ratio in dichloromethane/acetonitrile mixture and with AgBr in dichloromethane afforded the corresponding mononuclear phosphine complexes $[\{(CuI)_2\}\{\{(o-PPh_2)C_6H_4\}C(O)NH(C_{12}H_{18})\}_2-\kappa^1-P]$ (3) and $[{(AgBr)_2}{\{(o-PPh_2)C_6H_4\}C(O)N(H)(C_{12}H_{18})\}_2-\kappa^1-P}]$ (4), in good yields. Further treatment of L1 with AgBF4 and AgClO4 in dichloromethane, in 1:1 ratio, yielded the complexes $[\{(AgX)_2\}]$ $\{\{(o-PPh_2)C_6H_4\}C(O)N(H)(C_{12}H_{18})\}_2-\kappa^3-P,O,C\}$ (X = BF₄ (5), ClO₄ (6)) as white solids in good yields (Scheme 4). The IR spectra

Table 1 Selected bond lengths (Å) and bond angles (°) of 1-2

	1	2
P1-Pd1	2.2096(14)	2.1787(8)
N1-Pd1	2.040(4)	2.014(2)
Pd1-Cl1	2.4549(14)	()
Pd1-Cl1′	2.3491(13)	
Pd1-O3	,	2.0413(18)
Pd1-O6		2.158(2)
N1-C7	1.337(6)	1.348(4)
C7-O1	1.231(6)	1.243(3)
O5-C65		1.280(3)
O3-C63		1.271(3)
Pd1-P1-N1	89.81(12)	88.87(7)
Cl1-Pd1-Cl1′	84.57(5)	
N1-Pd1-Cl1	93.23(12)	
P1-Pd1-Cl1	176.25(5)	
O3-Pd1-P1	,	90.91(6)
N1-Pd1-O3		175.43(8)
O6-Pd1-P1		176.35(6)
N1-Pd1-O6		94.54(8)



Scheme 4 Synthesis of Cu¹ and Ag¹ dimeric complexes 3–6.

showed N-H stretching frequencies at 3284 cm⁻¹ (5) and 3248 cm⁻¹ (6) and a common carbonyl stretching frequency at 1609 cm⁻¹. The structures of complexes 3-6 were unambiguously confirmed by single-crystal X-ray diffraction.

Perspective views are shown in Fig. 3, selected bond lengths and bond angles are mentioned in Table 2 for better comparison. Complexes 3–6 contain $\mathrm{Cu^I}$ and $\mathrm{Ag^I}$ centers, each adopting a distorted trigonal planar geometry. Complexes 3 and 4 are neutral species, while 5 and 6 are cationic, balanced by $\mathrm{ClO_4}^-$ and $\mathrm{BF_4}^-$ counterions, respectively. All four complexes exhibit tridentate coordination. In 3 and 4, the ligands coordinate through an η^1 -P donor mode, accompanied by bridging

halide ions, leading to the formation of four-membered metallacycles. In contrast, complexes 5 and 6 display P,O,C-tridentate coordination, resulting in the formation of two five-membered and one twelve-membered metallacycles.

Synthesis of amide based monophosphine ligand: *N*-(2,6-dibenzhydryl-4-methylphenyl)-2-(diphenylphosphaneyl) benzamide (L2)

The dialkylation of p-toluidine using diphenylmethanol as alkylating agent under solvent-free conditions, in stoichiometric amount of conc. HCl and ZnCl2 produced 2,6-dibenzhydryl-4-methylaniline, which upon further treatment with 2-bromobenzoyl chloride in 1:1 molar ratio afforded new amide derivative A. The treatment of amide derivative with 1.3 equiv. of diphenylphosphine in presence of catalytic amount of [Pd (PPh₃)₄] and K₂CO₃ yielded new monophosphine ligand L2 in high yield. In ¹H NMR spectrum, characteristics NH proton appeared at 7.29 ppm and in ¹³C{¹H} NMR spectrum carbonyl carbon appeared at 168.2 ppm. Aromatic protons showed resonance around 7–7.8 ppm. In IR spectrum the secondary amide band appeared at 3401 cm⁻¹ and the carbonyl stretching frequency appeared at 1684 cm⁻¹. Treatment of L2 with H₂O₂ in THF resulted in phosphine oxide 7 (Scheme 5). The structure 7 was confirmed by single crystal X-ray analysis and is shown in Fig. 4, with selected bond lengths and bond angles mentioned in the figure captions.

Synthesis of Cu^I and Ru^{II} complexes

Reaction of ligand L2 with CuI in 1:1 molar ratio in a dichloromethane/acetonitrile mixture yielded complex [{(CuI)₂} {{(o-PPh₂)C₆H₄}C(O)NH(C₃₃H₂₈)}₂- κ ¹-P] (8) as a yellow solid in good yield. The IR spectrum of 8 exhibited a secondary amide N–H stretching band at 3435 cm⁻¹ and a carbonyl stretching frequency at 1652 cm⁻¹. Treatment of ligand L2 with [Ru(p-cymene)Cl₂]₂ in the presence of NH₄PF₆ (1:1 molar ratio) under reflux in methanol afforded the cationic Ru complex [{(Ru(p-cymene)Cl)}{{(o-PPh₂)C₆H₄}C(O)NH(C₃₃H₂₈)}- κ ²-P,O] (PF₆) (9), isolated as an orange solid in good yield (Scheme 6).

Both complexes were crystallized by slow diffusion of petroleum ether into dichloromethane solutions of the respective compounds. The molecular structures of complexes 8 and 9 are shown in Fig. 5, with selected bond lengths and angles provided in the figure captions. In complex 8, both Cu^I centres

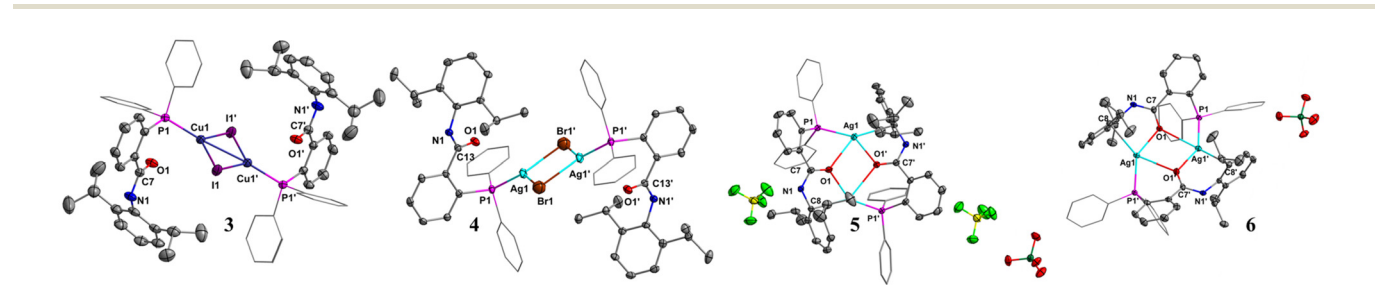


Fig. 3 Single X-ray crystal structure of complexes 3–6. All hydrogen atoms have been omitted for clarity. Displacement ellipsoids are drawn at 50% probability level.

Table 2 Selected bond lengths (Å) and bond angles (°) of 3-6

	3(X = I)(M = Cu)	4 (X = Br) (M = Ag)	5 (M = Ag)	6 (M = Ag)
P1-M1	2.2257(6)	2.4154(7)	2.3669(11)	2.3688(6)
M1-X1	2.5535(3)	2.6947(6)		
M1'-X1	2.5847(3)	2.6758(5)		
C8-M1			2.629(4)	2.633(2)
O1-M1			2.271(3)	2.2707(19)
M1-M1'	2.7235(5)	3.6989(10)		,
N1-C7	1.344(3)	1.357(3)	1.337(6)	1.332(3)
O1-C7	1.227(3)	1.230(3)	1.246(6)	1.247(3)
M1-X1-M1'	64.015(11)	87.062(16)	` ,	
X1-M1-X1'	115.987(11)	92.938(16)		
P1-M1-X1	127.309(18)	134.247 (18)		
P1-M1-X1'	115.794(18)	134.606(17)		
P1-M1-C8	. ,	` ,	148.05(10)	147.92(5)
O1-M1-P1			142.96(9)	142.99(5)

Scheme 5 Synthesis of ligand L2 and 7.

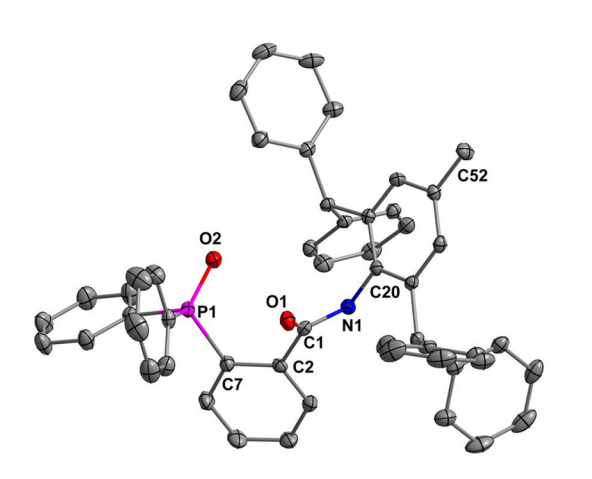
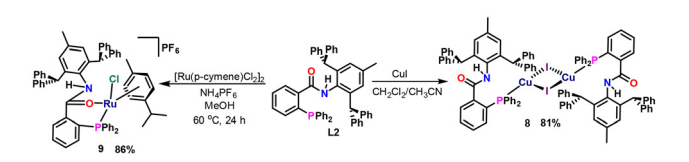


Fig. 4 Molecular structure of 7. All hydrogen atoms and solvent molecules have been omitted for clarity. Displacement ellipsoids are drawn at 50% probability level. Bond length(Å) and bond angles (°): P1-O2 1.4738 (17), P1-C7 1.823(2), O1-C1 1.220(3), N1-C20 1.435(3), N1-C1 1.350(3), O2-P1-C7 112.28(10), C1-N1-C20 123.57(18), O1-C1-N1 123.5(2), O1-C1-C2 122.12(19), N1-C1-C2 114.25(18).



Scheme 6 Synthesis of complexes 8 and 9.

adopt a distorted trigonal planar geometry. Complex 9 being a catanionic complex features Ru^{II} center in a distorted tetrahedral geometry, with PF₆ as a counter ion.

Structural insights from ³¹P{¹H} NMR spectroscopy

The coordination behaviour of the phosphine moiety in ligands L1 and L2 and their corresponding metal complexes was systematically examined using ³¹P{¹H} NMR spectroscopy. The free ligands L1 and L2 exhibited singlets at -11.4 ppm and -10.6 ppm, respectively, which are characteristic of uncoordinated tertiary phosphines. Upon coordination to PdII, the phosphorus signals shifted markedly downfield, with complex 1 displaying a singlet at 16.6 ppm and complex 2 at 26.3 ppm. These substantial downfield shifts reflect deshielding of the phosphorus nuclei due to coordination with the electrondeficient PdII center, and are consistent with P,N-chelation in a square planar environment.76,77 The further downfield shift observed in complex 2 compared to 1 may arise from the stronger electron-withdrawing effect of the acetate ligands relative to chlorides, enhancing the deshielding of the phosphorus atom.

In contrast, the Cu^I and Ag^I complexes derived from L1 (complexes 3-6) exhibited significantly upfield-shifted ³¹P signals. Complexes 3 and 4 displayed singlets at -6.1 ppm and -8.8 ppm, respectively, consistent with monodentate η^{1} -P coordination of the soft phosphine donor to the d^{10} Cu^I and Ag^I centers.⁷⁸ The upfield chemical shifts reflect reduced deshielding in the absence of strong π -backbonding and in a less electron-deficient coordination environment. Interestingly, complexes 5 and 6, which involve tridentate P,O,C

Paper Dalton Transactions

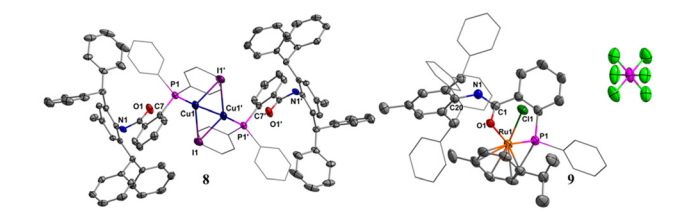


Fig. 5 Single X-ray crystal structure of complexes **8** and **9**. All hydrogen atoms have been omitted for clarity. Displacement ellipsoids are drawn at 50% probability level. Selected bond distances [Å] and bond angles [°]: for **8**: Cu1–I1 2.5827(5), Cu1′–I1 2.5588(6), Cu1–Cu1′ 2.6108(8), P1–Cu1 2.2260(9), N1–C7 1.356(4), O1–C7 1.222(3), Cu1–I1–Cu1′ 61.031(15), I1–Cu1–I1′ 118.969(15), I1–Cu1–Cu1′ 59.032(18), I1′–Cu1–Cu1′ 59.937(18), P1–Cu1–I1 123.47(3), P1–Cu1–I1′ 116.90(3), P1–Cu1–Cu1′ 171.16(3). For **9**: Ru1–Cl1 2.3868(12), Ru1–P1 2.3308(14), Ru1–O1 2.105(3), O1–C1 1.258(5), P1–Ru1–Cl1 88.05(5), O1–Ru1–Cl1 86.24(9), O1–Ru1–P1 79.69 (9).

coordination to $\mathrm{Ag^I}$, exhibited doublets at 10.9 ppm with $^1J_{\mathrm{P-Ag}}$ value of 756.5 and 753.3 Hz, respectively. These doublets confirm direct coordination of phosphorus to the Ag center and reflect a stronger interaction in the more rigid tridentate coordination mode, as well as increased covalency in the P-Ag bond.

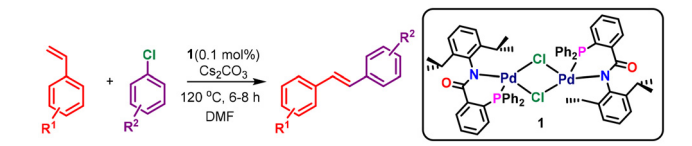
The Ru^{II} complex **9** derived from **L2** exhibited a 31 P{ 1 H} singlet at 32.5 ppm, indicating significant deshielding upon P, O-chelation to the electrophilic Ru^{II} center in a distorted tetrahedral geometry. Additionally, a septet observed at $^{-144.3}$ ppm corresponds to the PF $_{6}$ counterion, with a $^{1}J_{PF}$ coupling of 712.8 Hz, further confirming the presence of the hexafluorophosphate anion in the complex.

Collectively, these data illustrate that the ^{31}P chemical shifts are highly sensitive to the oxidation state, electron density, and coordination geometry of the metal center, as well as the denticity and rigidity of the ligand framework. Downfield shifts typically accompany coordination to more electron-deficient or π -accepting metals (Pd^{II} , Ru^{II}), while upfield shifts are observed with softer, less electronegative metal centers (Cu^{I} , Ag^{I}) in monodentate modes. The presence of P–Ag scalar coupling in complexes 5 and 6 further underscores the strong, covalent nature of the metal–phosphorus interaction in these systems. These results collectively highlight the versatility of amide-functionalized phosphines in modulating electronic environments through varied coordination modes across different metal centers.

Heck-coupling reaction between various aryl chlorides and styrene derivatives promoted by P,N-Pd^{II} complex 1

Chlorobenzene and styrene were selected as model substrates to optimize the reaction conditions. No product formation was observed in the absence of either the catalyst or the base (Table 3, entries 1 and 2). Using 0.05 mol% of catalyst 1 afforded an 83% yield of *trans*-stilbene, which increased to 99% upon increasing the catalyst loading to 0.1 mol% (entries 3 and 4). Among the bases tested, Cs₂CO₃ proved most effective (entries 4–7), and DMF was identified as the optimal solvent (entries 4 and 8–10). Lowering the reaction tempera-

Table 3 Optimization of the reaction condition for Heck-coupling reaction



Entry	Catalyst	Solvent	Base	Yield ^a (%)
1	No catalyst	DMF	Cs ₂ CO ₃	NC
2	1	DMF	No base	NC
3^b	1	DMF	Cs_2CO_3	83
4	1	DMF	Cs_2CO_3	99
5	1	DMF	NaOH	74
6	1	DMF	Na_2CO_3	86
7	1	DMF	KO ^t Bu	73
8	1	Toluene	Cs_2CO_3	54
9	1	DMSO	Cs_2CO_3	69
10	1	THF	Cs_2CO_3	61
11 ^c	1	DMF	Cs_2CO_3	58

^a Yield determined by GC-MS. NC = no conversion. Chlorobenzene (0.50 mmol), styrene (0.6 mmol), Cs_2CO_3 (0.6 mmol), Pd cat 1 (0.1 mol%) and solvent (2 mL), 120 °C. ^b Catalyst loading (0.05 mol%). ^c Reaction temp = 80 °C.

ture to 80 °C resulted in diminished yield (entry 11). The optimal conditions-0.1 mol% catalyst 1, Cs_2CO_3 as base, and DMF as solvent at 120 °C (entry 4), were adopted for further substrate scope evaluation (Scheme 7).

Under these conditions, a wide range of activated aryl chlorides coupled efficiently with styrene, affording the corresponding *trans*-stilbenes in excellent yields (90–99%). *ortho*-,

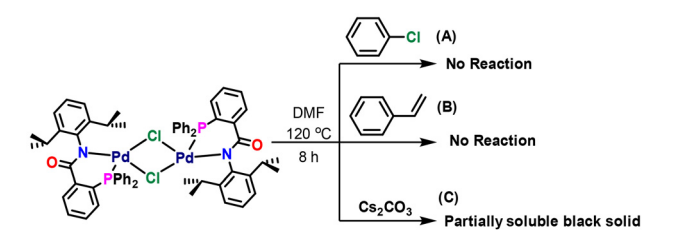
Scheme 7 Substrate scope Heck-coupling reaction. Conditions: aryl chloride (0.50 mmol), styrene (0.60 mmol), Cs_2CO_3 (0.60 mmol), DMF 2 mL, 120 °C, and catalyst 1 (0.1 mol%). All are isolated yields.

Dalton Transactions Paper

meta-, and para-substituted aryl chlorides bearing both electron-donating and electron-withdrawing groups were well tolerated. Notably, heteroaryl chlorides such as 2-chloronaphthalene and 2-chlorothiophene also participated effectively, providing the desired products in 90% and 92% yields, respectively (Scheme 7, entries \mathbf{k} and \mathbf{r}).

To investigate the reaction pathway, stoichiometric reactions of complex 1 with chlorobenzene and styrene were conducted in DMF (Scheme 8). In case of A and B, even upon heating the reaction mixture to 120 °C, no visible colour change was observed. When a mixture of complex 1, Cs₂CO₃, and DMF was heated in a catalytic tube at 120 °C (C), a grevish suspension formed. A similar greyish suspension was observed after 6 hours in a reaction tube containing all the reactants (Fig. 6).

To confirm the nature of the catalytic process, mercury drop and CS2 poisoning test were conducted, indicating a heterogeneous mechanism likely involving Pd nanoparticles derived from complex 1. Scanning electron microscopy images (Fig. 7(a) and (b)) revealed irregularly shaped particles in residues obtained from both (a) the reaction of complex 1 with Cs₂CO₃ and (b) the model catalytic reaction. These residues were isolated by DMF evaporation, followed by sequential washing with methanol, CH2Cl2, water, and methanol. The Pd nanoparticles exhibited average sizes ranging from 30-80 nm.



Scheme 8 Mechanistic investigation of trans-stilbene formation [(A) reaction of complex 1 with chlorobenzene, (B) reaction of complex 1 with styrene, and (C) reaction of complex 1 with Cs₂CO₃].

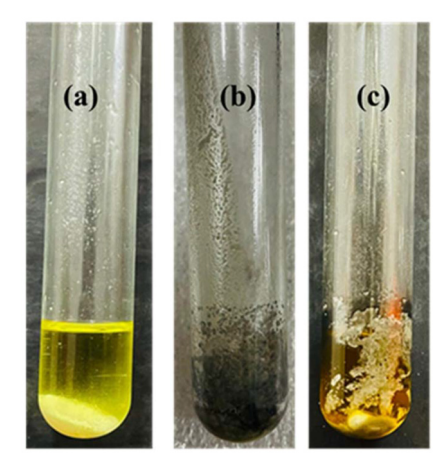


Fig. 6 (a) Catalyst 1 and Cs_2CO_3 , (b) catalyst 1 and Cs_2CO_3 upon heating at 120 °C. (c) Reaction mixture after 6 h.

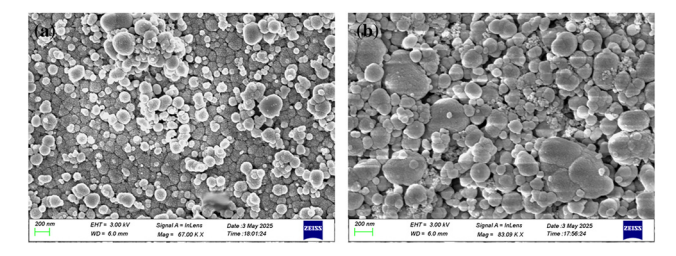


Fig. 7 (a) SEM image of catalyst 1 and Cs₂CO₃. (b) SEM image of the catalytic reaction residue.

EDX elemental mapping (Fig. S103†) confirmed the presence of C, P, N, O and Pd, supporting the stabilization of Pd NPs by ligand L1 and the reductive role of Cs₂CO₃. To verify that the nanoparticles are indeed stabilized by the parent ligand L1 and not by decomposition products, we conducted comparative FT-IR spectroscopic analysis of free ligand L1, complex 1, and the isolated Pd nanoparticles. In the IR spectrum of ligand L1, characteristic bands were observed at 3364 cm⁻¹ (ν_{N-H}) and 1653 cm⁻¹ $(\nu_{C=O})$, corresponding to the amide functionalities. Upon coordination to PdII in complex 1, the ν_{N-H} band disappeared and the $\nu_{C=0}$ band shifted to 1601 cm⁻¹, clearly indicating coordination of the amide nitrogen to the metal center. For the Pd nanoparticles, IR analysis revealed the presence of both ν_{N-H} (3465 cm⁻¹) and $\nu_{C=0}$ (1666 cm⁻¹) bands, closely resembling those of the parent ligand (Fig. 8). This observation strongly supports the retention of ligand L1 on the nanoparticle surface, suggesting that L1 acts as a stabilizing agent. The absence of new or shifted functional group frequencies also suggests that no major ligand decomposition has occurred during nanoparticle formation. These IR results, in conjunction with the EDX elemental mapping, which confirms the presence of P, N, O, and Pd, provide strong evidence that the Pd nanoparticles are indeed stabilized by the intact ligand L1.

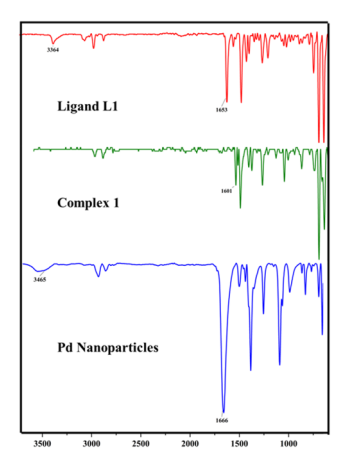


Fig. 8 IR spectra of red (ligand L1), green (complex 1) and blue (Pd nanoparticles).

Paper **Dalton Transactions**

Scheme 9 A plausible mechanism for the Heck-coupling reaction between aryl chlorides and styrene derivatives.

Catalyst recyclability was evaluated over five cycles. After each run, the catalyst was recovered by solvent removal, washed, dried at 100 °C, and reused. Yields remained ≥90% under optimal conditions throughout the cycles. SEM analysis after the fifth cycle (Fig. S104†) showed no significant changes in particle size or aggregation, underscoring the stability and robustness of the Pd nanoparticles. Furthermore, the practicality of the catalytic system was demonstrated through a gramscale reaction, which afforded 97% yield of product a.

A plausible catalytic mechanism for the Heck coupling reaction is proposed based on experimental evidence and supported by literature 48,79-81 (Scheme 9). Catalyst 1 acts as a Pd⁰ reservoir, with Cs₂CO₃ facilitating it's in situ reduction to Pd⁰ nanoparticles. The Pd nanoparticles are stabilized by ligand L1 and Cs₂CO₃ acts as a reductant for complex 1. The catalytic cycle begins with oxidative addition of the Pd⁰ species into the aryl or alkenyl halide (R-X) bond, followed by alkene insertion into the resulting Pd-Ar intermediate. Subsequent synβ-hydride elimination affords the trans-stilbene product. Finally, elimination of hydrogen halide and its neutralization by the base regenerate the active Pd⁰ species, completing the cycle.

Conclusions

In summary, we have successfully synthesized and characterized two novel sterically hindered amide-based monophosphine ligands, L1 and L2, and explored their coordination chemistry with a range of transition metals, including Pd¹¹,

Cu^I, Ag^I, and Ru^{II}. Among the resulting complexes, the dimeric P,N-coordinated palladium complex 1 exhibited outstanding catalytic performance in the Heck cross-coupling of aryl chlorides with styrene derivatives. The in situ generation of stabilized Pd nanoparticles from complex 1, facilitated by the hemilabile P,N ligand and base-induced reduction, was confirmed through SEM analysis and mercury and CS2 poisoning tests, supporting a heterogeneous catalytic mechanism. This catalytic system operated efficiently under mild conditions with low catalyst loadings (0.1 mol%), delivering trans-stilbene products in high yields (90-99%) and displaying excellent substrate scope and recyclability. These results highlight the potential of sterically encumbered P,N-type ligands in stabilizing catalytically active nanoparticles and enabling practical, selective, and sustainable C-C bond-forming transformations.

Experimental section

Instrumentation

NMR spectra were recorded on Bruker FT spectrometers (Avance-400 or 500) MHz at ambient probe temperatures. ¹³C {1H} and 11P{1H} NMR spectra were acquired using a broad band decoupling method. The spectra were recorded in CDCl₃ and DMSO- d_6 solutions with TMS as an internal standard; chemical shifts of ¹H and ¹³C{¹H} NMR spectra are reported in ppm downfield from TMS. The chemical shifts of ³¹P{¹H} NMR spectra are referred to 85% H₃PO₄ as an external standard. Positive values indicate downfield shifts. Mass spectra were recorded using Bruker Maxis Impact LC-q-TOF mass spectrometer. Infrared spectra were recorded on a PerkinElmer Spectrum One FT-IR spectrometer (model no. 73465) in KBr disk. GC-MS analyses were performed on an Agilent 7890A GC system with an FID detector using a J & W DB-1 column (10 m, 0.1 mm ID). The melting points of all compounds were determined on a Veego melting point apparatus and are uncorrected. Analytical TLC was performed on a Merck 60F254 silica gel plate (0.25 mm thickness), and column chromatography was performed on Merck (100-200 MESH). The morphological studies of the thin films were conducted with a field emission scanning electron microscope (FE-SEM, JSM-7600F).

General procedure for the Mizoroki-Heck coupling reaction

The reactions were performed in a closed vessel containing a mixture of aryl halide (1 equiv.), styrene (1.2 equiv.), Cs₂CO₃ (1.2 equiv.), catalyst 1 (0.1 mol%) and 2 mL DMF. The reaction vessel was placed into an oil bath and heated at 120 °C. After completion of the reaction, the crude reaction mixture was treated with water (20 mL) and ethyl acetate (20 mL). The organic layer was washed with 2 × 10 mL H₂O, dried over Na₂SO₄. The solvent was removed under reduced pressure, and the resulting crude product was purified by column chromatography on neutral or basic alumina.

Synthesis of $\{(o-PPh_2)C_6H_4C(O)N(H)(C_{12}H_{18})\}$ (L1). To a thick-walled seal tube containing a magnetic stir bar were added 2-bromo-N-(2,6-diisopropylphenyl)benzamide (1 g,

2.775 mmol), Pd(PPh₃)₄ (0.192 g, 0.166 mmol, 6 mol%), K₂CO₃ (0.421 g, 3.053 mmol, 1.1 equiv.), toluene (10 mL), and PPh₂H (0.671 g, 3.608 mmol, 1.3 equiv.). The tube was sealed and heated to 150 °C for 24 h with vigorous stirring. After 24 h, the reaction mixture was cooled, diluted with dichloromethane (40 mL), and washed with distilled water (3 × 30 mL). The organic layer was dried over anhydrous Na2SO4 and filtered, and the solution was concentrated under vacuum to give L1 a white colour solid, which was purified by flash chromatography over silica, eluting with 3:7 ethyl acetate/pet ether. The monophosphine L1 was characterized by multinuclear NMR spectroscopy and mass spectroscopy. Yield 75% (0.950 g). Mp: 158 °C. ¹H NMR (400 MHz, CDCl₃) δ 7.95 (ddd, J = 7.6, 3.8, 1.3 Hz, 1H), 7.62-7.55 (m, 2H), 7.52-7.40 (m, 7H), 7.39-7.33 (m, 5H), 7.25 (d, J = 7.7 Hz, 2H), 7.14 (dt, J = 7.7, 2.5 Hz, 1H), 3.25 (hept, J = 6.8 Hz, 2H), 1.22 (d, J = 6.9 Hz, 12H). ³¹P{¹H} NMR (162 MHz, CDCl₃) δ –11.4(s). ¹³C(¹H) NMR (101 MHz, CDCl₃) δ $168.5(s) \ 146.5(s), \ 136.8(d, J = 11 \ Hz), \ 135.2(s), \ 134.8(s) \ 134(s),$ 133.8(s), 131(s), 130.7(s), 129.4(s), 129(s), 128.9(s), 128.8(d, J =7 Hz) 128.5(s), 123.6(s), 28.9(s), 23.9(s). HRMS (ESI), m/z: calcd for $C_{31}H_{33}N_1P_1O_1$ [M + H]⁺: 466.2294; found 466.2272. Anal. calcd for C₃₁H₃₂NOP: C, 79.97; H, 6.93; N, 3.01. Found: C, 79.94; H, 6.90; N, 3.03. FT-IR (KBr disk, cm⁻¹): 3364 (ν_{NH}) s, 2962 s, 2865 w, 1653 s ($\nu_{\rm CO}$), 1515 s, 1301 m, 746 s, 698 s.

Synthesis of $[\{(PdCl)_2\}\{\{(o-PPh_2)C_6H_4\}C(O)N(C_{12}H_{18})\}_2-\kappa^2-P,$ N] (1). Ligand L1 (0.05 g, 0.107 mmol) in 10 mL dichloromethane was added to a solution of [PdCOD(Cl)₂] (0.036 g, 0.107 mmol) in 10 mL dichloromethane. The reaction mixture was allowed to stir at room temperature for 6 h. The solvent was completely removed under reduced pressure to afford complex 1 as yellow solid. The resulting solid was washed with petroleum ether (2 × 20 mL) to afford analytically pure complex 1. Yield: 83% (0.108 g). Mp: 195 °C. ¹H NMR (400 MHz, CDCl₃) δ 8.67 (s, 2H), 7.89 (s, 4H), 7.73 (d, J = 7.6 Hz, 3H), 7.48 (t, J = 7.7 Hz, 4H), 7.37 (t, J = 7.8 Hz, 3H), 7.25 (d, J = 8.2 Hz, 8H, 7.16 (d, J = 7.6 Hz, 3H), 6.91 (s, 5H), 6.62 (s, 5H)2H), 2.66 (s, 4H), 0.86 (s, 24H). ³¹P{¹H} NMR (162 MHz, CDCl₃) δ 16.6(s). HRMS (ESI), m/z: calcd for $C_{31}H_{31}CINOPPd [M + H]^+$: 606.0939; 608.0937. found Anal. C₆₂H₆₂Cl₂N₂O₂P₂Pd₂: C, 61.40; H, 5.15; N, 2.31. Found: C, 61.38; H, 5.59; N, 2.45. FT-IR (KBr disk, cm⁻¹): 3070, 2959 m, 2853 w, 1540 m ($\nu_{\rm CO}$), 1462 m, 1323 s, 1102 s.

Synthesis of [{(CH₃C(O)O)(Pd)₂}{{(o-PPh₂)C₆H₄}C(O)N (C₁₂H₁₈)}₂-κ²-*P*,*N*] (2). Ligand L1 (0.05 g, 0.107 mmol) in 10 mL dichloromethane was added to a solution of Pd(OAc)₂ (0.024 g, 0.107 mmol) in 10 mL dichloromethane. The reaction mixture was allowed to stir at room temperature for 6 h. The solvent was completely removed under reduced pressure to afford complex 2 as yellow solid. The resulting solid was washed with petroleum ether (2 × 20 mL) to afford analytically pure complex 2. Yield: 85% (0.114 g). Mp: 182–184 °C. ¹H NMR (400 MHz, CDCl₃) δ 8.46–8.43 (m, 1H), 7.67–7.43 (m, 24H), 7.33 (d, J = 7.6 Hz, 2H), 7.19 (d, J = 7.8 Hz, 2H), 7.07 (d, J = 7.6 Hz, 3H), 6.78 (dd, J = 12.3, 7.6 Hz, 2H), 3.08–2.90 (m, 4H), 1.16–0.73 (m, 30H). ¹³C{¹H} NMR (101 MHz, CDCl₃) δ 181.3(s), 164(s), 146.4(s), 145(s), 134.1(d, J = 12 Hz) 133.8(s), 132.9(d, J =

9 Hz), 132.5(s), 131.4(s), 129.8(d, J = 9 Hz), 129.4(d, J = 12 Hz), 126.9(s), 126.60(s), 126(s), 123.5(s), 122.6(s), 29(s), 24.5(s), 24.2(s). ³¹P{¹H} NMR (202 MHz, CDCl₃) δ 26.3(s). HRMS (ESI), m/z: calcd for $C_{33}H_{35}N_1P_1O_3Pd_1$ [M + H]⁺: 630.1384; found 630.1418. Anal. calcd for $C_{66}H_{68}N_2O_6P_2Pd_2$: C, 62.91; H, 5.44; N, 2.22. Found: C, 61.38; H, 5.19; N, 2.33. FT-IR (KBr disk, cm⁻¹): 2961 s, 2865 w, 1549 m (ν CO), 1438 w, 1263 s, 1099 s, 805 s

Synthesis of $[\{(CuI)_2\}\{\{(o-PPh_2)C_6H_4\}C(O)NH(C_{12}H_{18})\}_2 - \kappa^2 - P$, N (3). CuI (0.005 g, 0.026 mmol) was suspended in acetonitrile (10 mL) and a solution of L1 (0.012 g, 0.026 mmol) in dichloromethane was added. The solution was stirred for 4 h producing a clear solution. The solution was filtered, and the solvent was removed under vacuum and residue obtained was washed with pet ether and dried to give 3 as a yellow solid. Crystals suitable for X-ray structure determination were grown by slow diffusion of pet ether into a saturated solution of the material in dichloromethane giving yellow crystals. Yield: 83% (0.116 g). Mp: 220–222 °C. 1 H NMR (400 MHz, CDCl₃) δ 7.86 (d, J = 7.3 Hz, 1H), 7.64-7.44 (m, 6H), 7.40-7.32 (m, 3H),7.27–7.19 (m, 5H), 7.08 (d, J = 7.7 Hz, 2H), 6.87 (t, J = 7.9 Hz, 1H), 2.78 (s, 2H), 0.95 (d, J = 6.8 Hz, 12H). ¹³C{¹H} NMR (101 MHz, CDCl₃) δ 167.7(s), 146.6(s), 146.2(s), 134.4(d, J = 16Hz), 132.7(s), 132.6(s), 132.5(s), 130.2(s), 130(s), 129.1(s), 128.9 (d, J = 9 Hz), 128.4(s), 127.9(s), 123.6(s), 123.4(s), 28.8(s),24.1(s). ³¹P{¹H} NMR (162 MHz, CDCl₃) δ -6.1(s). HRMS (ESI), m/z: calcd for $C_{31}H_{32}N_1P_1O_1Cu_1$ [M - I]⁺: 528.1512; found 528.1513. Anal. calcd for C₆₂H₆₄Cu₂I₂N₂O₂P₂: C, 56.75; H, 4.92; N, 2.14. Found: C, 56.79; H, 4.96; N, 2.17. FT-IR (KBr disk, cm⁻¹): 3053 (ν_{NH}) s, 2963 s, 2870 w, 1615 s (ν_{CO}), 1508 s, 1097 w, 748 s.

Synthesis of $[{(a_2Br)_2}{\{(o-PPh_2)C_6H_4\}C(O)N(H)(C_{12}H_{18})\}_2}$ κ^{1} -P] (4). Ligand L1 (0.05 g, 0.107 mmol) in 10 mL dichloromethane was added to a solution of AgBr (0.020, 0.107 mmol) in 10 mL dichloromethane. The reaction mixture was allowed to stir at room temperature for 6 h. The solvent was completely removed under reduced pressure to afford complex 4 as white solid. The resulting solid was washed with petroleum ether (2 × 20 mL) to afford analytically pure complex 4. Yield: 86% (0.120 g). Mp: 237–239 °C. 1 H NMR (400 MHz, CDCl₃) δ 7.85 (s, 1H), 7.52-7.09 (m, 17H), 7.01 (d, J = 10.1 Hz, 1H), 3.08 (s, 2H), 1.10 (s, 12H). $^{13}C\{^{1}H\}$ NMR (126 MHz, CDCl₃) δ 168.3(s), 146.5(s), 134.9(s), 134(s), 133.9(s), 131(s), 130.8(s), 129.6(s), 129.3(s), 128.9(s), 128.9(s), 128.8(s), 128.5(s), 123.7(s), 28.9(s), 23.9(s). ³¹P{¹H} NMR (162 MHz, CDCl₃) δ -8.8(s). HRMS (ESI), m/z: calcd for $C_{31}H_{32}N_1P_1O_1Ag_1 [M - Br]^+$: 572.1267; found 572.1266. Anal. calcd for C₆₂H₆₄Ag₂Br₂N₂O₂P₂: C, 56.99; H, 4.94; N, 2.14. Found: C, 56.95; H, 4.92; N, 2.11. FT-IR (KBr disk, cm⁻¹): 3318 (ν_{NH}) s, 2964 s, 2869 w, 1652 s (ν_{CO}), 1506 s, 1260 s, 1100 m, 800 s, 746 s, 696 s.

Synthesis of $[\{(AgBF_4)_2\}\{\{(o-PPh_2)C_6H_4\}C(O)N(H)(C_{12}H_{18})\}_{2}-\kappa^3-P,O,C]$ (5). Ligand L1 (0.05 g, 0.107 mmol) in 10 mL dichloromethane was added to a solution of $AgBF_4$ (0.020, 0.107 mmol) in 10 mL dichloromethane. The reaction mixture was allowed to stir at room temperature for 6 h. The solvent was completely removed under reduced pressure to afford

Paper **Dalton Transactions**

complex 5 as white solid. The resulting solid was washed with petroleum ether (2 × 20 mL) to afford analytically pure complex 5. Yield: 81% (0.114 g). Mp: 236-238 °C. ¹H NMR (400 MHz, DMSO) δ 9.61 (s, 2H), 7.87 (s, 2H), 7.78 (s, 1H), 7.59-7.26 (m, 3H), 7.34-6.65 (m, 22H), 6.65 (d, J = 7.7 Hz, 3H), 6.38 (s, 2H), 6.20 (s, 1H), 2.28-2.09 (m, 4H), 1.11 to -0.31 (m, 24H). ³¹P{¹H} NMR (162 MHz, DMSO) δ 10.9 (d, J = 758.3 Hz). ¹³C{¹H} NMR (101 MHz, DMSO) δ 167.7(s), 146.6(s), 139.6(s), 134.2(d, J = 17 Hz), 133.2(s), 132.9(s), 132.4(d, J = 19 Hz), 131.4(d, J = 19 Hz), 130.1(s), 129.8(s), 129.2(s), 128.6(s), 128(s),123.5(s), 79.6(s), 28.6(s), 23.5(s). HRMS (ESI), m/z: calcd for $C_{31}H_{32}N_1P_1O_1Ag_1$ [M]⁺: 572.1267; found 572.1267. Anal. calcd for C₆₂H₆₄Ag₂B₂F₈N₂O₂P₂: C, 56.39; H, 4.88; N, 2.12. Found: C, 56.42; H, 4.84; N, 2.15. FT-IR (KBr disk, cm⁻¹): 3284 (ν_{NH}) s, 2971 s, 2872 w, 1609 s ($\nu_{\rm CO}$), 1519 s, 1310 w, 1087 s, 749 s, 695 s.

Synthesis of $[\{(AgClO_4)_2\}\{\{(o-PPh_2)C_6H_4\}C(O)N(H)(C_{12}H_{18})\}_{2}$ κ^3 -P,O,C] (6). Ligand L1 (0.05 g, 0.107 mmol) in 10 mL dichloromethane was added to a solution of AgClO₄ (0.022, 0.107 mmol) in 10 mL dichloromethane. The reaction mixture was allowed to stir at room temperature for 6 h. The solvent was completely removed under reduced pressure to afford complex 6 as white solid. The resulting solid was washed with petroleum ether (2 × 20 mL) to afford analytically pure complex 6. Yield: 82% (0.118 g). Mp: 224-226 °C. ¹H NMR (400 MHz, DMSO) δ 10.01 (s, 2H), 8.32 (d, J = 7.7 Hz, 2H), 7.77 (t, J = 7.6 Hz, 4H), 7.60 (t, J = 7.7 Hz, 4H), 7.35 (s, 14H), 7.20 (t, J = 7.6 Hz, 4H), 7.60 (t, J = 7.7 Hz, 4H), 7.35 (s, 14H), 7.20 (t, J = 7.6 Hz, 4H), 7.35 (s, 14H), 7.20 (t, J = 7.6 Hz, 4H), 7.35 (s, 14H), 7.20 (t, J = 7.6 Hz, 4H), 7.35 (s, 14H), 7.20 (t, J = 7.6 Hz, 4H), 7.35 (s, 14H), 7.3J = 7.7 Hz, 4H), 7.06 (d, J = 7.7 Hz, 6H), 2.58-2.53 (m, 4H), 0.88-0.73 (m, 24H). $^{31}P{^{1}H}$ NMR (162 MHz, CDCl₃) δ 10.9 (d, $^{1}J_{PAg}$ 753.3). $^{13}C\{^{1}H\}$ NMR (101 MHz, DMSO) δ 166.9(s), 146(s), 135.6(s), 133.8(s), 133.6(s), 133(s), 132.1(s), 131.8(s), 130.8(s), 130.6(s), 129.5(s), 129.1(s), 127.9(s), 122.9(s), 79.2(s), 28(s), 22.9(s). HRMS (ESI), m/z: calcd for $C_{31}H_{32}N_1P_1O_1Ag_1$ [M]⁺: 572.1261; found 572.1267. Anal. calcd C₆₂H₆₄Ag₂Cl₂N₂O₁₀P₂: C, 55.33; H, 4.79; N, 2.08. Found: C, 55.37; H, 4.34; N, 2.05. FT-IR (KBr disk, cm⁻¹): 3248 (ν_{NH}) s, 2963 s, 2866 w, 1609 s ($\nu_{\rm CO}$), 1516 s, 1310 w, 1084 s, 917 s, 748 s, 697 s.

Synthesis of $\{(o-PPh_2)C_6H_4C(O)N(H)(C_{33}H_{28})\}$ (L2). To a thick-walled seal tube containing a magnetic stir bar were 2-bromo-N-(2,6-dibenzhydryl-4-methylphenyl)benzamide (1 g, 1.606 mmol), Pd(PPh₃)₄ (0.111 g, 0.096 mmol, 6 mol%), K₂CO₃ (0.244 g, 1.766 mmol, 1.1 equiv.), toluene (10 mL), and PPh₂H (0.388 g, 2.08 mmol, 1.3 equiv.). The tube was sealed and heated to 150 °C for 24 h with vigorous stirring. After 24 h, the reaction mixture was cooled, diluted with dichloromethane (40 mL), and washed with distilled water (3 × 30 mL). The organic layer was dried over anhydrous Na₂SO₄ and filtered, and the solution was concentrated under vacuum to give L2 a white colour solid, which was purified by flash chromatography over silica, eluting with 3:7 ethyl acetate/pet ether. The monophosphine L2 was characterized by multinuclear NMR spectroscopy and mass spectroscopy. Yield 82% (0.950 g). Mp: 205 °C. 1 H NMR (400 MHz, CDCl₃) δ 7.35–7.14 (m, 32H), 6.95 (dd, J = 7.4, 3.6 Hz, 1H), 6.57 (d, J = 2.8 Hz, 3H), 6.33 (d, J = 3.1 Hz, 1H), 5.99 (s, 2H), 2.10 (s, 3H). ¹³C{¹H} NMR

(101 MHz, CDCl₃) δ 168.3(s), 143.6(s), 142.1(s), 137.6(s), 137.3(s), 134.9(s), 133.8(s), 133.6(s), 130.9(s), 130.1(s), 129.6(s), 128.6-128.3(m), 126.5(s), 126.3(s), 51.9(s), 21.7(s). ${}^{31}P\{{}^{1}H\}$ **NMR** (162 MHz, CDCl₃) δ –10.6(s). HRMS (ESI), m/z: calcd for $C_{52}H_{43}N_1P_1O_1[M+H]^+$: 728.3077; found 728.3073. Anal. calcd for C₅₂H₄₂NOP: C, 85.81; H, 5.82; N, 1.92. Found: C, 85.84; H, 5.84; N, 1.93. FT-IR (KBr disk, cm⁻¹): 3401 (ν_{NH}) s, 3061 m, 3026 w, 1684 s ($\nu_{\rm CO}$), 1482 s, 1031 m, 753 s.

Synthesis of $\{(o-OPPh_2)C_6H_4C(O)N(H)(C_{33}H_{28})\}$ (7). H_2O_2 (1 mL, 3.089 mmol, 30% H₂O₂) was added to a solution of L2 (0.050 g, 0.107 mmol) in THF (30 mL) and stirred at room temperature for 12 h. After removing the solvents under reduced pressure, the sticky oil obtained was washed with petroleum ether $(2 \times 20 \text{ mL})$ to give analytically pure compound 7 as a white solid. Single-crystals of 7 suitable for X-ray analysis were obtained by slow diffusion of petroleum ether into the dichloromethane solution of 7. Yield: 80% (0.064 g). ¹H NMR (400 MHz, CDCl₃) δ 7.31-7.17 (m, 25H), 7.05 (d, J = 5.1 Hz, 8H), 6.97-6.93 (m, 1H), 6.57 (s, 2H), 6.34 (s, 1H), 5.98 (s, 2H), 2.11 (s, 3H). ¹³C{¹H} NMR (101 MHz, CDCl₃) δ 168.2(s), 143.6(s), 142.1(s), 137.7(d, J = 12 Hz) 137.3(s), 134.9(s), 133.8(s), 133.6(s), 130.9(s), 130.1(s), 129.6(s), 128.6(m), 126.5(d, J = 5 Hz), 126.3(s), 51.9(s), 21.6(s). ³¹P{¹H} NMR (162 MHz, CDCl₃) δ 32.8(s). HRMS (ESI), m/z: calcd for C₅₂H₄₃N₁P₁O₂ [M + H]⁺: 744.3028; found 744.3027. Anal. calcd for $C_{52}H_{42}NO_2P$: C, 83.96; H, 5.69; N, 1.88. Found: C, 83.99; H, 5.71; N, 1.86. FT-IR (KBr disk, cm⁻¹): 3404 (ν_{NH}) w, 3041 w, 1679 s (ν_{CO}), 1462 m, 1264 m, 1094 w, 760 s.

Synthesis of $[\{(CuI)_2\}\{\{(o-PPh_2)C_6H_4\}C(O)NH(C_{33}H_{28})\}_2-\kappa^1-P]$ (8). CuI (0.005 g, 0.026 mmol) was suspended in acetonitrile (10 mL) and a solution of L2 (0.018 g, 0.026 mmol) in dichloromethane was added. The solution was stirred for 4 h producing a clear solution. The solution was filtered, and the solvent was removed under vacuum and residue obtained was washed with pet ether and dried to give 8 as a yellow solid. Crystals suitable for X-ray structure determination were grown by slow diffusion of pet ether into a saturated solution of the material in dichloromethane giving yellow crystals. Yield: 81% (0.159 g). Mp: 228-230 °C. HRMS (ESI), m/z: calcd for $C_{52}H_{42}N_1P_1O_1Cu_1$ [M - I]⁺: 790.2295; found 790.2258. Anal. calcd for C₁₀₄H₈₄Cu₂I₂N₂O₂P₂: C, 68.01; H, 4.61; N, 1.53. Found: C, 68.05; H, 4.63; N, 1.56. FT-IR (KBr disk, cm⁻¹): 3435 $(\nu_{\rm NH})$ s, 3056 w, 3023 w, 1662 s $(\nu_{\rm CO})$, 1493 m, 1284 w, 1240 w, 744 m, 702 s. ³¹P{¹H} NMR (162 MHz, CDCl₃) δ –18.4(s).

Synthesis of $[{(Ru(p-cymene)Cl)}{(o-PPh_2)C_6H_4}C(O)NH$ $(C_{33}H_{28})-\kappa^2-P,O$ (PF₆) (9). Ligand L2 (0.05 g, 0.107 mmol) and NH₄PF₆ (0.017 g, 0.107 mmol) in 10 mL methanol was added to a solution of $[Ru(p\text{-cymene})Cl_2]_2$ (0.032, 0.0535 mmol) in 10 mL methanol. The reaction mixture was refluxed at 60 °C for 24 h. The reaction mixture was filtered through Celite and the solvent was completely removed under reduced pressure to afford complex 9 as orange solid. The resulting solid was washed with diethyl ether (2 × 20 mL) to afford analytically pure complex 9. Yield: 86% (0.105 g). ¹H NMR (400 MHz, CDCl₃) δ 9.43 (s, 1H), 8.36 (s, 1H), 7.77 (dd, J = 11.8, 7.6 Hz, 2H), 7.69-7.43 (m, 11H), 7.29 (s, 9H), 7.12 (dd, J = 7.8, 1.4 Hz,

1H), 6.85 (dd, I = 11.4, 7.6 Hz, 1H), 5.83 (d, I = 5.5 Hz, 1H), 5.59 (d, J = 5.8 Hz, 1H), 5.48 (d, J = 5.6 Hz, 1H), 5.23 (d, J = 5.6 Hz, 1H)Hz, 1H), 1.36 (d, J = 6.6 Hz, 3H), 0.80 (d, J = 6.9 Hz, 3H), 0.74 (d, J = 6.8 Hz, 3H), 0.65 (d, J = 6.2 Hz, 3H). ³¹P{¹H} NMR (162 MHz, CDCl₃) δ 32.5, -144.3 (sept, ${}^{1}J_{PF}$ 714.4 Hz). ${}^{13}C\{{}^{1}H\}$ **NMR** (101 MHz, CDCl₃) δ 170.8(s), 146.1(s), 145.9(s), 134.6(d, J = 11 Hz), 133.4(d, J = 9 Hz), 132.9-132.3(m), 131.9(s), 131.3(s), 131.2(s), 130.7(s), 129.9(d, J = 9 Hz), 129.3(d, J = 11 Hz), 129(s), 128.9(s), 128.7(s), 128.5(s), 128.1(s), 126.9(s), 123.4(d, J = 3 Hz), 104.3(s), 100(s), 88.8(s), 87.8(s), 86.9(s), 86.8(s), 29.1(s), 28.8(s), 24.6(s), 23.2(s), 20.2(s), 16.9(s). Anal. C₆₂H₅₆ClF₆NOP₂Ru: C, 65.12; H, 4.94; N, 1.22. Found: C, 65.16; H, 4.38; N, 1.32. FT-IR (KBr disk, cm⁻¹): 3397 (ν_{NH}) w, 3070 w, 2493 w, 1597 m ($\nu_{\rm CO}$), 1519 w, 1442 w, 1323 w, 1259 w, 1102 w, 838 s, 704 s.

Author contributions

The manuscript was written through contributions of all authors. All authors have given approval to the final version of the manuscript.

Conflicts of interest

There are no conflicts to declare.

Data availability

The data supporting this article have been included as part of the ESI.†

ESI contents: crystal structure determination of compounds; NMR and HRMS spectra of complexes; controlled experiments of reaction mechanism; NMR and mass spectra of catalytic products.

Acknowledgements

MSB thank Indian Institute of Technology Bombay for supporting this work through Research Development Fund (RDF). We are thankful to the Department of Chemistry, IIT Bombay, for instrumentation facilities, as well as spectral and analytical data. GS acknowledges the financial support from IITB and KCD thanks UGC for the fellowship.

References

- 1 Y. Canac, Chem. Rec., 2023, 23, e202300187.
- 2 M. R. Tiddens and M.-E. Moret, in *Metal-Ligand Co-operativity: Catalysis and the Pincer-Metal Platform*, ed. G. van Koten, K. Kirchner and M.-E. Moret, Springer International Publishing, Cham, 2021, pp. 25–69.
- 3 S. Maggini, Coord. Chem. Rev., 2009, 253, 1793-1832.

- 4 K. N. Gavrilov and A. I. Polosukhin, *Russ. Chem. Rev.*, 2000, 69, 661–682.
- 5 P. J. Guiry and C. P. Saunders, Adv. Synth. Catal., 2004, 346, 497–537.
- 6 L. Radhakrishna, B. S. Kote, H. S. Kunchur, M. K. Pandey, D. Mondal and M. S. Balakrishna, *Dalton Trans.*, 2022, 51, 5480–5493.
- 7 M. P. Carroll and P. J. Guiry, Chem. Soc. Rev., 2014, 43, 819–833
- 8 L. Alig, M. Fritz and S. Schneider, *Chem. Rev.*, 2019, **119**, 2681–2751.
- 9 J. Bae and E. J. Cho, ACS Catal., 2023, 13, 13540-13560.
- 10 H. S. Kunchur, L. Radhakrishna, M. K. Pandey and M. S. Balakrishna, Chem. Commun., 2021, 57, 4835–4838.
- 11 H. S. Kunchur and M. S. Balakrishna, *Inorg. Chem.*, 2022, **61**, 857–868.
- 12 B. Michelet, D. Lebœuf, C. Bour, K. Škoch, F. Horký, P. Štěpnička and V. Gandon, *ChemPlusChem*, 2017, 82, 442–448.
- 13 B. T. Ingoglia and S. L. Buchwald, Org. Lett., 2017, 19, 2853–2856.
- 14 B. V. Rokade and P. J. Guiry, ACS Catal., 2018, 8, 624-643.
- 15 M. K. Yılmaz, S. İnce, M. Keleş and B. Güzel, *J. CO2 Util.*, 2020, 42, 101309.
- 16 B. S. Kote, M. A. Mohite, D. Mondal, M. K. Pandey and M. S. Balakrishna, *Eur. J. Inorg. Chem.*, 2023, 26, e202300291.
- 17 J. I. van der Vlugt, J. M. J. Paulusse, E. J. Zijp, J. A. Tijmensen, A. M. Mills, A. L. Spek, C. Claver and D. Vogt, *Eur. J. Inorg. Chem.*, 2004, 2004, 4193–4201.
- 18 A. Aghmiz, A. M. Masdeu-Bultó, C. Claver and D. Sinou, *J. Mol. Catal. A: Chem.*, 2002, **184**, 111–119.
- 19 F. Schneck, M. Finger, M. Tromp and S. Schneider, *Chem. Eur. J.*, 2017, 23, 33–37.
- 20 R. González-Fernández, P. Crochet and V. Cadierno, *Dalton Trans.*, 2020, **49**, 210–222.
- 21 D. G. A. Verhoeven and M.-E. Moret, *Dalton Trans.*, 2016, 45, 15762–15778.
- 22 M. K. Pandey, J. T. Mague and M. S. Balakrishna, *Inorg. Chem.*, 2018, 57, 7468–7480.
- 23 R. Gourkhede, B. Kaur, B. S. Kote and M. S. Balakrishna, *Dalton Trans.*, 2024, 53, 10693–10703.
- 24 M. R. Tiddens, B. T. Kappé, T. J. Smak, M. Lutz and M.-E. Moret, *Chem. Eur. J.*, 2024, **30**, e202400666.
- 25 S. S. Ng, Z. Chen, O. Y. Yuen and C. M. So, *Org. Biomol. Chem.*, 2022, **20**, 1373–1378.
- 26 W.-M. Dai and Y. Zhang, *Tetrahedron Lett.*, 2005, **46**, 1377–1381.
- 27 X. F. Bai, T. Song, Z. Xu, C. G. Xia, W. S. Huang and L. W. Xu, Angew. Chem., 2015, 127, 5344–5348.
- 28 W.-M. Dai, K. K. Y. Yeung, J.-T. Liu, Y. Zhang and I. D. Williams, *Org. Lett.*, 2002, **4**, 1615–1618.
- 29 W.-M. Dai, Y. Li, Y. Zhang, C. Yue and J. Wu, *Chem. Eur. J.*, 2008, **14**, 5538–5554.
- 30 M. H. Tse, P. Y. Choy and F. Y. Kwong, *Acc. Chem. Res.*, 2022, 55, 3688–3705.

Paper

31 W. Li and J. Zhang, Acc. Chem. Res., 2024, 57, 489-513.

- 32 N. W. Boaz, J. A. Ponasik, S. E. Large and S. D. Debenham, *Tetrahedron: Asymmetry*, 2004, **15**, 2151–2154.
- 33 M. Tamizmani, R. Kankanala and C. Sivasankar, J. Organomet. Chem., 2014, 763–764, 6–13.
- 34 B. Tezcan, M. Kemal Yılmaz, G. Yakalı, M. Aygün and B. Güzel, *Inorg. Chim. Acta*, 2022, **543**, 121155.
- 35 L. Yin and J. Liebscher, Chem. Rev., 2007, 107, 133-173.
- 36 K. A. Jantan, G. Ekart, S. McCarthy, A. J. P. White, D. C. Braddock, A. Serpe and J. D. E. T. Wilton-Ely, *Catalysts*, 2024, 14, 295.
- 37 E. A. Onoabedje and U. C. Okoro, *Synth. Commun.*, 2019, 49, 2117–2146.
- 38 A. Biffis, P. Centomo, A. Del Zotto and M. Zecca, *Chem. Rev.*, 2018, **118**, 2249–2295.
- 39 N. Selander and K. J. Szabó, *Chem. Rev.*, 2011, **111**, 2048–2076.
- 40 R. Taakili, C. Barthes, C. Lepetit, C. Duhayon, D. A. Valyaev and Y. Canac, *Inorg. Chem.*, 2021, **60**, 12116–12128.
- 41 A. Balanta, C. Godard and C. Claver, *Chem. Soc. Rev.*, 2011, **40**, 4973–4985.
- 42 Z. Wang, P. Xiao, B. Shen and N. He, *Colloids Surf.*, *A*, 2006, 276, 116–121.
- 43 A. Bej, K. Ghosh, A. Sarkar and D. W. Knight, *RSC Adv.*, 2016, **6**, 11446–11453.
- 44 K. Hong, M. Sajjadi, J. M. Suh, K. Zhang, M. Nasrollahzadeh, H. W. Jang, R. S. Varma and M. Shokouhimehr, ACS Appl. Nano Mater., 2020, 3, 2070– 2103.
- 45 J. Wang, W. S. Cheon, J.-Y. Lee, W. Yan, S. Jung, H. W. Jang and M. Shokouhimehr, *Dalton Trans.*, 2023, 52, 3567–3574.
- 46 S. Ince, Ö. Öner, M. K. Yılmaz, M. Keleş and B. Güzel, *Inorg. Chem.*, 2023, **62**, 4637–4647.
- 47 M. Tamura and H. Fujihara, *J. Am. Chem. Soc.*, 2003, **125**, 15742–15743.
- 48 S. Sheokand and M. S. Balakrishna, *Inorg. Chem.*, 2023, **62**, 12317–12328.
- 49 S. McCarthy, D. C. Braddock and J. D. E. T. Wilton-Ely, Coord. Chem. Rev., 2021, 442, 213925.
- 50 M. Alaqarbeh, S. F. Adil, T. Ghrear, M. Khan, M. Bouachrine and A. Al-Warthan, *Catalysts*, 2023, 13, 1343.
- 51 C. Deraedt and D. Astruc, Acc. Chem. Res., 2014, 47, 494-503.
- 52 F. Ulusal, E. Erünal and B. Güzel, *J. Nanopart. Res.*, 2018, **20**, 219.
- 53 P. J. Anju, M. Neetha and G. Anilkumar, *ChemistrySelect*, 2022, 7, e202103564.
- 54 R. F. Heck and J. Nolley Jr, *J. Org. Chem.*, 1972, **37**, 2320–2322.
- 55 K. S. Madden, S. David, J. P. Knowles and A. Whiting, *Chem. Commun.*, 2015, **51**, 11409–11412.
- 56 S. Mohanty and M. S. Balakrishna, *J. Chem. Sci.*, 2010, **122**, 137–142.

- 57 S. Mohanty, D. Suresh, M. S. Balakrishna and J. T. Mague, *Tetrahedron*, 2008, **64**, 240–247.
- 58 D. Mondal and M. S. Balakrishna, Eur. J. Inorg. Chem., 2020, 2020, 2392-2402.
- 59 I. P. Beletskaya and A. V. Cheprakov, *Chem. Rev.*, 2000, **100**, 3009–3066.
- 60 O. Blacque and C. M. Frech, *Chem. Eur. J.*, 2010, **16**, 1521–1531.
- 61 M. Oberholzer and C. M. Frech, *Green Chem.*, 2013, **15**, 1678–1686.
- 62 D. Mc Cartney and P. J. Guiry, Chem. Soc. Rev., 2011, 40, 5122–5150.
- 63 M. Oberholzer and C. M. Frech, *J. Visualized Exp.*, 2014, e51444, DOI: 10.3791/51444.
- 64 K. Hirabayashi, Y. Nishihara, A. Mori and T. Hiyama, *Tetrahedron Lett.*, 1998, **39**, 7893–7896.
- 65 K. Kikukawa and T. Matsuda, Chem. Lett., 1977, 6, 159-162.
- 66 Y. Hou, J. Ma, H. Yang, E. A. Anderson, A. Whiting and N. Wu, *Chem. Commun.*, 2019, 55, 3733–3736.
- 67 M. Beller, H. Fischer, W. A. Herrmann, K. Öfele and C. Brossmer, Angew. Chem., Int. Ed. Engl., 1995, 34, 1848– 1849.
- 68 S. Jagtap, Catalysts, 2017, 7, 267.
- 69 V. W. Bhoyare, E. D. Sosa Carrizo, C. C. Chintawar, V. Gandon and N. T. Patil, *J. Am. Chem. Soc.*, 2023, 145, 8810–8816.
- 70 S. Mukhopadhyay, G. Rothenberg, A. Joshi, M. Baidossi and Y. Sasson, *Adv. Synth. Catal.*, 2002, **344**, 348–354.
- 71 H.-J. Xu, Y.-Q. Zhao and X.-F. Zhou, *J. Org. Chem.*, 2011, 76, 8036–8041.
- 72 W. A. Herrmann, C. Brossmer, C.-P. Reisinger, T. H. Riermeier, K. Öfele and M. Beller, *Chem. Eur. J.*, 1997, 3, 1357–1364.
- 73 W. Chen, I. Shaikh, F. Ahmed, S. Karkoub, M. AlRawashdeh, H. Zhou and S. Madrahimov, *ChemistryOpen*, 2024, **13**, e202300249.
- 74 N. Kvasovs, V. Iziumchenko, V. Palchykov and V. Gevorgyan, ACS Catal., 2021, 11, 3749–3754.
- 75 S. Lerch, S. Fritsch and T. Strassner, *Eur. J. Org. Chem.*, 2022, e202200008.
- 76 G. Sabharwal, K. C. Dwivedi, C. Das, T. R. K. Rana, A. Dutta, G. Rajaraman and M. S. Balakrishna, *J. Catal.*, 2024, 440, 115825.
- 77 K. C. Dwivedi, G. Sabharwal, B. S. Kote and M. S. Balakrishna, *Dalton Trans.*, 2024, 53, 18321–18329.
- 78 K. C. Dwivedi, G. Sabharwal, A. Pandey and M. S. Balakrishna, *Inorg. Chem.*, 2025, **64**, 10989–11000.
- 79 J. P. Knowles and A. Whiting, *Org. Biomol. Chem.*, 2007, 5, 31–44.
- 80 V. P. W. Böhm and W. A. Herrmann, *Chem. Eur. J.*, 2001, 7, 4191–4197.
- 81 A. M. Trzeciak and J. J. Ziółkowski, *Coord. Chem. Rev.*, 2005, **249**, 2308–2322.